

Article

FeF₃/(Acetylene Black and Multi-Walled Carbon Nanotube) Composite for Cathode Active Material of Thermal Battery through Formation of Conductive Network Channels

Su Hyeong Kim ^{1,†}, Ji-Hyeok Choi ^{1,†} , So Hyun Park ¹, Tae Young Ahn ², Hae-Won Cheong ^{2,*} 
and Young Soo Yoon ^{1,*} 

¹ Department of Materials Science & Engineering, Gachon University, Seongnam 13120, Republic of Korea; kkd1573@gachon.ac.kr (S.H.K.); joshua9456@gachon.ac.kr (J.-H.C.); psh6575@gachon.ac.kr (S.H.P.)
² Agency for Defense Development (ADD), Daejeon 34186, Republic of Korea; ahnty@add.re.kr
* Correspondence: hwcheong@add.re.kr (H.-W.C.); benedicto@gachon.ac.kr (Y.S.Y.)
† These authors contributed equally to this work.

Abstract: Considerable research is being conducted on the use of FeF₃ as a cathode replacement for FeS₂ in thermal batteries. However, FeF₃ alone is inefficient as a cathode active material because of its low electrical conductivity due to its wide bandgap (5.96 eV). Herein, acetylene black and multi-walled carbon nanotubes (MWCNTs) were combined with FeF₃, and the ratio was optimized. When acetylene black and MWCNTs were added separately to FeF₃, the electrical conductivity increased, but the mechanical strength decreased. When acetylene black and MWCNTs were both added to FeF₃, the FeF₃/M₁AB₄ sample (with 1 wt.% MWCNTs and 4% AB) afforded a discharge capacity of approximately 74% of the theoretical capacity (712 mAh/g) of FeF₃. Considering the electrical conductivity and mechanical strength, this composition was confirmed to be the most suitable.

Keywords: thermal battery; FeF₃; cathode active material; multi-walled carbon nanotube; acetylene black



Citation: Kim, S.H.; Choi, J.-H.; Park, S.H.; Ahn, T.Y.; Cheong, H.-W.; Yoon, Y.S. FeF₃/(Acetylene Black and Multi-Walled Carbon Nanotube) Composite for Cathode Active Material of Thermal Battery through Formation of Conductive Network Channels. *Nanomaterials* **2023**, *13*, 2783. <https://doi.org/10.3390/nano13202783>

Academic Editors: Zhibin Wu and Yirong Zhu

Received: 3 October 2023

Revised: 12 October 2023

Accepted: 16 October 2023

Published: 17 October 2023

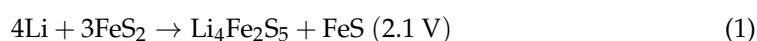


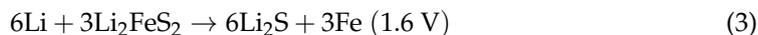
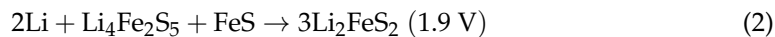
Copyright: © 2023 by the authors. Licensee MDPI, Basel, Switzerland. This article is an open access article distributed under the terms and conditions of the Creative Commons Attribution (CC BY) license (<https://creativecommons.org/licenses/by/4.0/>).

1. Introduction

A thermal battery is a reserve-type battery that uses molten salt as an electrolyte and is activated at high temperatures (generally 350–550 °C) by heating when its use as a primary battery is required [1–3]. Thermal batteries can be stored for a long time; therefore, they are used as a power source for guided missiles in the military or as a power source for hydraulic systems in aircraft for emergency purposes [4,5]. Thermal batteries have developed rapidly in recent years, aiming to ensure stability and reliability when used as an energy storage device in extreme environments (vibration, shock, acceleration, and pressure). The main physical and chemical characteristics required for the active cathode materials of thermal batteries are high thermal stability, high electronic conductivity, low solubility in molten electrolytes, low equivalent weight, good discharge kinetics, and reasonable cost [6,7].

Simply stated, the electrolyte in a thermal battery exists in a salt state with low reactivity at room temperature, which blocks contact between the anode and cathode. In this state, the movement of Li⁺ ions is controlled, and the self-discharge is kept low, enabling long-term storage. When the use of the battery is required, the user supplies heat by activating an ignitor, which liquefies the electrolyte and supplies power through an electrochemical reaction. The most commonly used thermal batteries employ Li-Si as the anode, iron disulfide (FeS₂) as the cathode, and LiCl-KCl (or three components) as the electrolyte. FeS₂ has the advantages of high conductivity in batteries, low cost, and a high theoretical capacity [8–10]. The reaction equations for a thermal battery using Li-Si as the anode and FeS₂ as the cathode are as follows [11]:





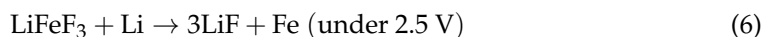
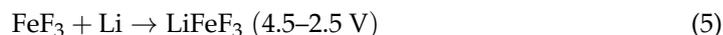
Among these materials, FeS_2 , a core material, decomposes into Fe_7S_8 or S_2 in the operating environment of thermal batteries, i.e., 550°C , lowering the discharge capacity [12,13]. The sulfur gas formed in the decomposition process seriously impacts the battery cathode and battery components and carries the risk of short circuits or battery explosions, raising safety issues [14].

Military equipment has become smarter with the recent development of cutting-edge defense technologies. Advancements have increased the precision and range of conventional artillery shells. Currently, a high-output power source that can overcome the spatial constraints of applications such as missiles and ensure miniaturization and precision is required. Therefore, there is an increasing need to develop new active cathode materials to solve the problems associated with FeS_2 in thermal batteries.

Currently, research on chlorides (NiCl_2) [15–17], fluorides (FeF_3 , NiF_2) [18,19], and oxides as next-generation active cathode materials for thermal batteries is in progress [20,21]. Among them, transition metal fluorides (TMFs) have attracted significant interest in academia [22]. TMFs have a high theoretical capacity owing to their multielectron conversion mechanism [23].



The reaction of iron fluoride (FeF_3), a type of TMF, proceeds via a two-step lithium (Li) intercalation and conversion reaction, affording a high theoretical capacity of 712 mAh/g.



The Li intercalation reaction proceeds between 4.5 V and 2.5 V, and the conversion reaction proceeds below 2.5 V [24]. FeF_3 has a theoretical capacity of 712 mAh/g, which is lower than that of FeS_2 , but has an energy density of 1947 Wh/kg, which is higher than that of FeS_2 (1273 Wh/kg) [25]. Additionally, FeF_3 is a candidate as a non-sulfide-based cathode active material due to its high-temperature stability above 550°C . However, FeF_3 has low electrical conductivity because of its wide bandgap (5.96 eV), and LiF, the product of the conversion reaction, is an insulator [26,27]. Therefore, the use of FeF_3 alone as an active cathode material in thermal batteries is inefficient.

In this study, multi-walled carbon nanotubes (MWCNTs), a carbon material widely used as a conductive material, and acetylene black (AB) were combined with FeF_3 in a composite to overcome the conductivity limitations of FeF_3 . The respective composites of AB and MWCNTs with FeF_3 exhibit improved electrical conductivity, but the durability of the pelletized FeF_3 composite was relatively low owing to the spring-back effect and agglomeration of the carbon materials. Spring-back is the geometric change made to a part at the end of the forming process when the part has been released from the forces of the forming tool. In the case of MWCNTs, this is an effect in which MWCNTs, pressed due to the pressure applied during the pelletizing process, try to return to their original state after the pressure is released. To solve this problem, a composite was fabricated by mixing AB and MWCNTs with FeF_3 in an appropriate ratio. When the FeF_3 composite was fabricated using only MWCNTs, the MWCNTs were not located between the FeF_3 particles. Therefore, a uniform conductive network could not be formed; the same was true for AB. When an FeF_3 composite was produced with AB and MWCNTs, the possibility of forming a conductive network between all FeF_3 particles increased, and the durability of the pelletized FeF_3 composite could be secured. The details are shown in Figure 1. The goal was to develop an organic binder-free cathode active material that overcame the

low electrical conductivity of FeF_3 for use as a high-density, high-voltage cathode active material in thermal batteries.

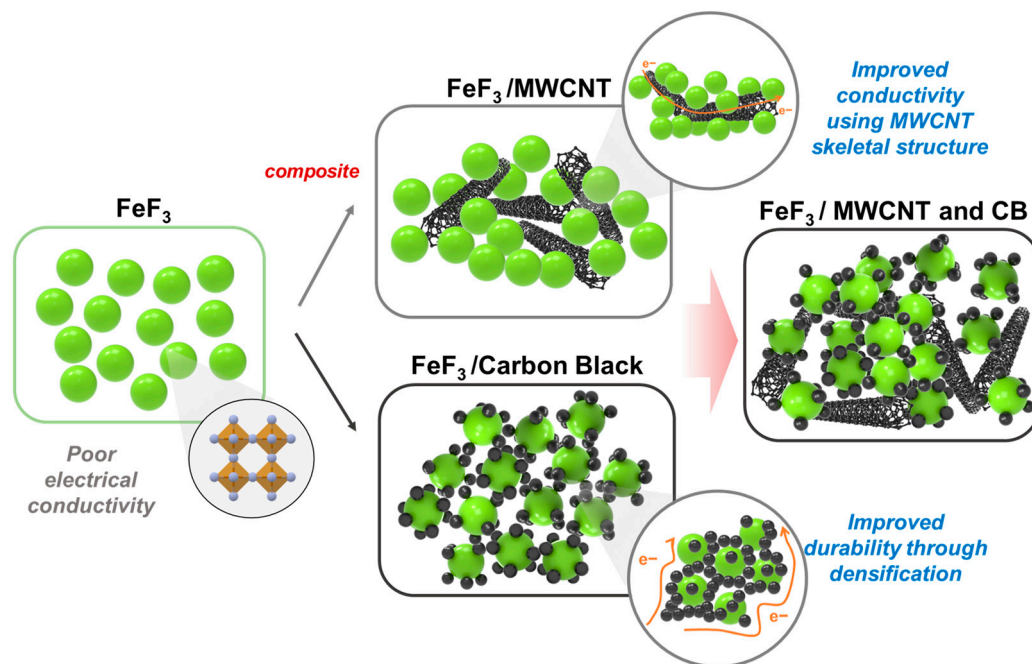


Figure 1. Schematic diagram of the mechanism for improving conductivity and durability through the addition of acetylene black and MWCNT.

2. Materials and Methods

2.1. Reagents

Iron fluoride (FeF_3 , Sigma-Aldrich, St. Louis, MO, USA), iron disulfide (FeS_2 , Alpha-Aesar, Haverhill, MA, USA), multiwalled carbon nanotubes (COOH-functionalized MWCNTs, US Research Nanomaterials, Houston, TX, USA), acetylene black (Graphene Supermarket, Ronkonkoma, NY, USA), and absolute ethanol (SAMCHUN, Pyungtaek, Republic of Korea) were used without additional purification.

2.2. Experimental Details

To fabricate the FeF_3 composite, FeF_3 , AB, and the MWCNTs were weighed in a ball-milling pot according to their respective weight ratios. The mixture was subjected to low-speed ball milling using 10 mm and 5 mm zirconia balls (powder: zirconia ball = 1:7 wt%). The ball-milled FeF_3 composite was used as a slurry for coin cell fabrication. Additional samples were dried and pelletized to measure the resistance, electrical conductivity, and mechanical strength. All experiments were conducted in a dry laboratory at 20% humidity, and the coin cells were assembled in a glove box under an argon environment. Owing to the difficulties in measuring the cathode discharge capacity in a thermal battery environment, the discharge capacity was measured in the laboratory using a half-cell with a Li metal (anode) and LiPF_6 (electrolyte).

2.3. Characterization

The effectiveness of the acid treatment of the MWCNTs was confirmed by Raman spectroscopy (Olympus, Tokyo, Japan, BX51), and the phase change of FeF_3 was identified by X-ray diffraction (XRD, Rigaku, SmartLab, Eagle Farm, Australia) after low-speed ball milling. The morphology of the samples was observed using a scanning electron microscope (SEM, Hitachi, Tokyo, Japan, SU8600), and the distribution of the elements was confirmed by energy-dispersive X-ray spectroscopy (EDS) analysis. Through thermogravimetric analysis (TGA, TA Instruments, New Castle, DE, USA, SDT Q600), the

high-temperature stability was determined from the weight change versus the temperature profile of each sample, and the activation energy was calculated. The TGA was analyzed from room temperature to 800 °C, at a temperature increase rate of 10 °C/min, and in the N₂ atmosphere. The battery discharge capacity was analyzed using a battery cycler (WonATech, Seoul, Republic of Korea, WBCS3000S). The discharge capacity was measured at a c-rate of 0.1 C, and the cutoff voltage was set at 0.5 V. The sheet resistance and specific resistance were measured using a four-point probe (Keithley, Cleveland, OH, USA, 2450 source meter) [28] and multi-meter probe (Fluke, Everett, DC, USA, 287 True RMS Multimeter), and the mechanical strength was measured using a compressive strength meter (ZwickRoell, Ulm, Germany, Z100SN). The sheet resistance of the pelletized active material was measured with a four-point probe, and the resistance in the horizontal and vertical directions of the pellet was measured with a multi-meter probe to confirm the tendency of the two results. The electrical conductivity was calculated using resistance measured with a four-point probe. The mechanical strength was measured using a 3 N load cell, and the maximum load was measured by setting the pellet vertically on the lower jig and lowering the upper jig at a speed of 5 mm/min. The pellet used at this time was manufactured with a diameter of 12 mm by applying a pressure of 30 kN.

3. Results

Figure 2a shows the TGA data for bare FeF₃ and FeS₂. FeS₂ was stable, showing a weight loss rate of approximately 2.5% up to 450 °C, followed by rapid decomposition, with a weight loss rate of approximately 25% at 700 °C. On the other hand, FeF₃ continued to lose weight even when the weight loss due to moisture (up to 250 °C) was excluded. However, there was no rapid decrease in the weight loss with increasing temperature, where the weight loss rate at 700 °C was ~10%, indicating better thermal stability compared with FeS₂. Because the thermal decomposition of the cathode active material in a thermal battery operating environment was a critical drawback affecting the battery performance, FeF₃ was selected instead of FeS₂.

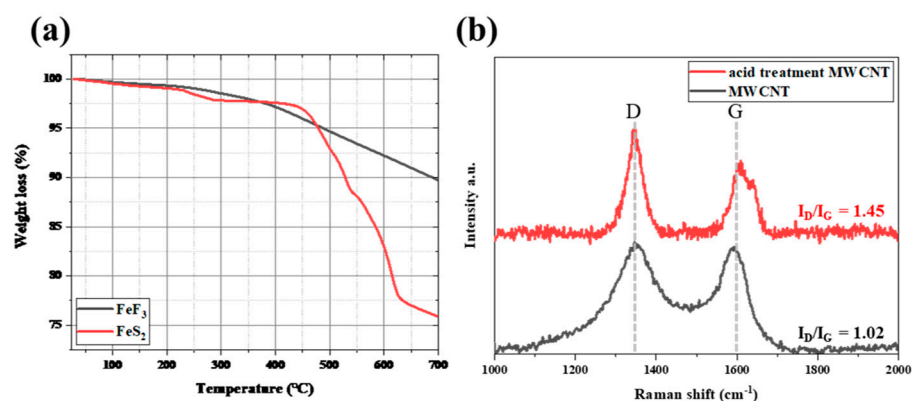


Figure 2. TGA data for FeS₂ and FeF₃ (a) and Raman spectra of the MWCNTs in the range of 1000–2000 cm⁻¹ (b).

Figure 2b shows the Raman spectra of the MWCNTs. The “D” peak reflects disorder in the MWCNTs, and the “G” peak is characteristic of carbon materials. The ratio of the intensity of the D peak to that of the G peak indicates the defect rate of the material. The I_D/I_G value of the MWCNTs was 1.02, and the I_D/I_G of the acid-treated MWCNTs was 1.45. The defect rate increased as the value of I_D/I_G increased; thus, the acid-treated MWCNTs had more defects. The acid-treated MWCNTs were more easily dispersed through the low-speed ball-milling process for producing a slurry of the samples for fabricating coin cells. In the COOH-functionalized MWCNTs, the π-conjugation was disrupted, and a surface dipole moment was introduced, which increased the dispersibility in solution [29,30]. To prepare the FeF₃/MWCNT composite, ethanol was added during mechanical dispersion via low-speed ball milling. Increasing the dispersibility of the MWCNTs was an important

factor for the fabrication of the $\text{FeF}_3/\text{MWCNT}$ composites. Therefore, the acid-treated MWCNTs were used in this study.

Figure 3a shows the XRD data after mixing 20 wt% AB and MWCNTs, respectively, with FeF_3 via low-speed ball milling. Hereafter, the samples mixed with AB are referred to as FeF_3/AB , and the samples mixed with MWCNTs are termed FeF_3/M . Because the sample fabrication process involves mechanical mixing using low-speed ball milling, it is possible that the phase of FeF_3 may change. However, a comparison of the XRD pattern with ICDD 00-033-0647 confirmed that the FeF_3 phase was maintained and that the sample used in the experiment had the characteristics of FeF_3 . Figure 3b,c show the SEM and EDS images after mixing 20 wt% AB and MWCNTs, respectively, with FeF_3 via low-speed ball milling. FeF_3 initially had a rhombohedral shape but adopted a spherical shape after the ball-milling process [31]. As shown in Figure 3b, the particles of both AB and FeF_3 were spherical, although FeF_3 and AB could be distinguished via EDS mapping, which confirmed that AB was distributed throughout the composite. Figure 3c shows the composite of FeF_3 and the MWCNTs, where tubular MWCNTs were observed. Similar to AB, the MWCNTs were distributed throughout the composite, as confirmed through EDS mapping.

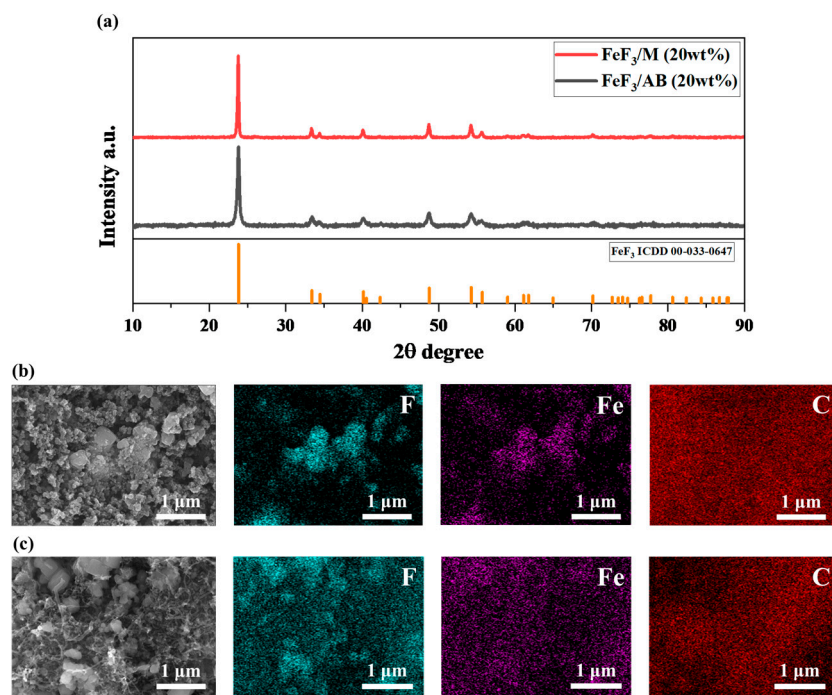


Figure 3. (a) XRD data for FeF_3 composites with 20 wt% AB and MWCNTs. SEM image of FeF_3 composite with 20 wt% AB (b) and MWCNTs (c).

Figure 4 shows the TGA data after mixing FeF_3 with up to 20 wt% AB and MWCNTs, with low-speed ball milling. The FeF_3/AB composites with 2.5, 5.0, 10.0, and 20.0 wt% AB showed 17%, 19%, 26%, and 25% weight loss up to 700 °C. The composites with 2.5, 5.0, 10.0, and 20.0 wt% MWCNTs showed weight loss rates of 8.7%, 10.8%, 13%, and 12.3%, respectively. The composites with AB underwent rapid weight loss after 400 °C, whereas the composites with the MWCNTs underwent a gradual weight loss after 550 °C. The weight loss before 250 °C was due to moisture evaporation, and the weight loss after 250 °C was due to the sublimation of AB and the MWCNTs. The composites with 10 wt% and 20 wt% AB showed a clear weight loss compared with the samples without AB. Because AB was thermally decomposed around 400 °C [32], the composites containing a greater amount of AB underwent greater weight loss. However, for all four composites with the MWCNTs, there was no significant difference in the weight loss. This was because the MWCNTs decomposed at a higher temperature than AB, that is, above 550 °C [33].

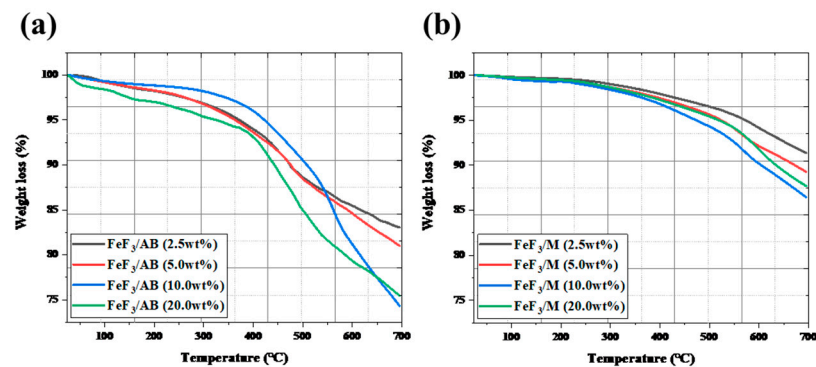


Figure 4. TGA data for FeF₃ composites of AB (a) and MWCNTs (b) in various ratios.

Table 1 shows the resistance, electrical conductivity, and mechanical strength of the composites, measured with a four-point probe and a multi-meter probe. As the amounts of added AB and MWCNTs increased, the resistance decreased, and the electrical conductivity increased. Unlike conventional batteries, thermal batteries use pelletized electrode materials. Therefore, good formability is required for pelletization. However, AB is agglomerated by van der Waals and electrostatic forces, making complete dispersion through mechanical processes difficult [34], whereas in the case of the MWCNTs, pelletization is difficult when pressure is applied owing to the spring-back effect [35]. This explains why the mechanical strength was not constant, as listed in Table 1. Therefore, the addition of AB and MWCNTs was optimized. The comparison of the electrical conductivity showed that the electrical conductivity was noticeably improved when both AB and the MWCNTs were added at 5 wt%. This was because 2.5 wt% of AB or MWCNT was insufficient to create a conductive network throughout the pellet; therefore, the particles acted as a resistance, whereas it was assumed that 5 wt% of AB or MWCNT was sufficient to create a conductive network throughout the pellet.

Table 1. Sheet resistance, vertical resistance, electrical conductivity, and mechanical strength of respective FeF₃ composites.

Type	Sheet Resistance (Ω/sq)	Multi-Meter Probe (Ω/mm)	Electrical Conductivity (S/m)	Mechanical Strength (MPa)
FeF ₃	2.590×10^6	Over-load	4.152×10^{-4}	0.2968
FeF ₃ /AB (2.5 wt%)	2.064×10^6	6091	6.291×10^{-4}	0.3723
FeF ₃ /AB (5.0 wt%)	312.9	2205	4.097	0.3175
FeF ₃ /AB (10.0 wt%)	14.78	49.19	76.91	0.2099
FeF ₃ /AB (20.0 wt%)	4.756	16.15	182.8	-
FeF ₃ /M (2.5 wt%)	1.249×10^6	105.3	8.090×10^{-4}	0.9007
FeF ₃ /M (5.0 wt%)	342.4	27.42	3.281	0.9301
FeF ₃ /M (10.0 wt%)	9.460	11.53	113.7	1.4189
FeF ₃ /M (20.0 wt%)	6.379	0.78	168.6	0.9975

Figure 5 shows the discharge capacity data for the composites with AB and MWCNTs in different ratios. The measured discharge capacity for the composites with 2.5, 5.0, 10.0, and 20.0 wt% AB was 414.5, 394.8, 389.4, and 363.1 mAh/g, respectively. The corresponding values for the composites with 2.5, 5.0, 10.0, and 20.0 wt% MWCNTs were 435.4, 452.9, 442.4, and 324.5 mAh/g, respectively. The discharge capacity was similar for all composites with AB, and only the composite with 20 wt% MWCNTs had a low discharge capacity. The composite with 5 wt% AB had a stable discharge profile, and the composite with

5 wt% MWCNTs had the highest discharge capacity. MWCNTs have been widely reported to have a higher electrical conductivity than carbon black (CB) [36,37]. However, as the amount of MWCNTs increased, the charge transfer rate decreased owing to aggregation of the MWCNTs [38]. When AB and MWCNTs were combined with FeF_3 , the electrical conductivity of the composite was improved at the expense of the capacity density because the amount of active material that could be contained in the battery was limited. Therefore, the amount of AB and MWCNTs added to FeF_3 was optimized. Considering the electrical conductivity, thermal stability, and discharge capacity, it was determined that adding 5 wt% AB or MWCNTs was optimal. The carbon material added to FeF_3 was fixed at 5 wt%. The AB and MWCNTs were mixed with FeF_3 in various ratios, and the resulting composites were analyzed.

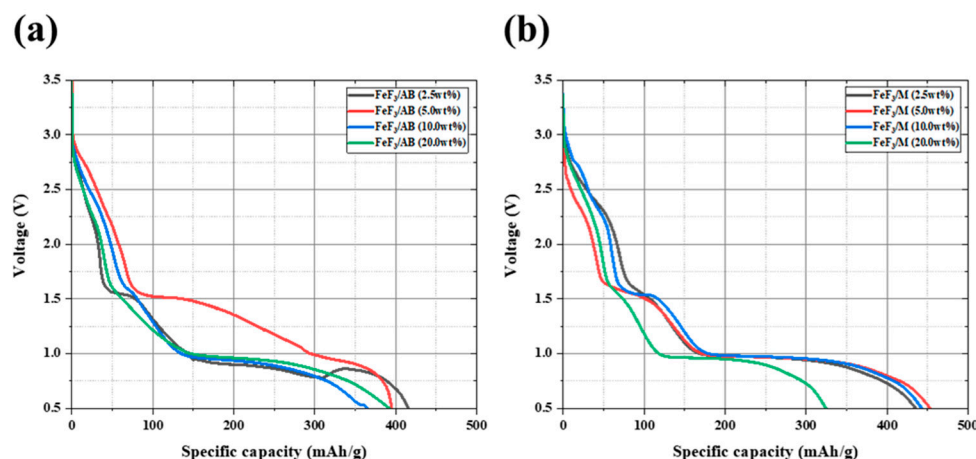


Figure 5. Discharge data for FeF_3 composite with AB (a) and MWCNT (b) at various ratios.

Figure 6 shows the TGA graph for the composite with a fixed carbon material to FeF_3 ratio of 5 wt%, where the ratios of the AB and MWCNTs were varied. Hereafter, the samples mixed with AB and MWCNTs at various ratios are denoted as $\text{FeF}_3/\text{M}(x\%)/\text{AB}(5-x\%)$. The weight loss rates up to 700 °C were 19.5%, 21%, 19.5%, and 15.7% for $\text{FeF}_3/\text{M}(1\text{ wt}\%)/\text{AB}(4\text{ wt}\%)$, $\text{FeF}_3/\text{M}(2\text{ wt}\%)/\text{AB}(3\text{ wt}\%)$, $\text{FeF}_3/\text{M}(3\text{ wt}\%)/\text{AB}(2\text{ wt}\%)$, and $\text{FeF}_3/\text{M}(4\text{ wt}\%)/\text{AB}(1\text{ wt}\%)$, respectively. Among the samples, $\text{FeF}_3/\text{M}(4\text{ wt}\%)/\text{AB}(1\text{ wt}\%)$, which had the highest MWCNT content, showed the lowest weight loss up to 700 °C. As explained above, because the MWCNTs had better thermal stability than AB, the sample with the highest MWCNT content had the lowest weight loss rate. The remaining samples exhibited similar weight loss rates without significant changes. However, at 550 °C, the operating temperature of the thermal battery, all samples were thermally stable with a weight loss rate of less than 10%.

Table 2 shows the resistance, electrical conductivity, and mechanical strength data after fixing the carbon material added to FeF_3 at 5 wt% and mixing the AB and MWCNTs at various ratios. The resistance and electrical conductivity were similar to or higher than those of the samples containing either AB or MWCNTs. The mechanical strength was also greatly improved compared with that of FeF_3 mixed with only AB or MWCNTs. Since the cathode active material of a thermal battery is used by pelletizing it through thermal compression, the mechanical strength characteristics of the pelletized cathode active material are an important factor. Therefore, presenting mechanical strength serves as a strength when compared with other studies [18]. The MWCNTs were randomly arranged between the FeF_3 particles, and empty spaces were inevitably formed between them. As AB entered this empty space, the empty space was reduced, and the packing density increased, thereby improving the mechanical strength of the pellet. This was attributed to the structural characteristics of the spherical AB and tube-shaped MWCNTs.

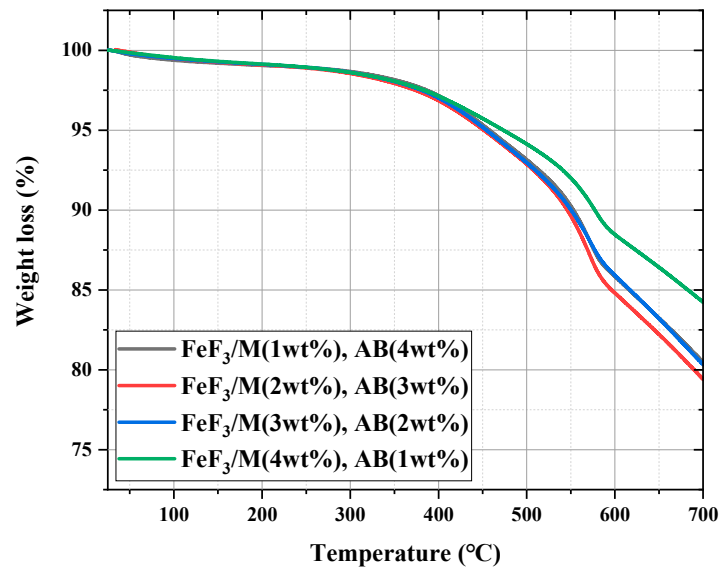


Figure 6. TGA data for FeF₃ composite with AB and MWCNTs at various ratios.

Table 2. Sheet resistance, vertical resistance, electrical conductivity, and mechanical strength of FeF₃/AB/MWCNT composites.

Type	Sheet Resistance (Ω/sq)	Multi-Meter Probe (Ω/mm)	Electrical Conductivity (S/m)	Mechanical Strength (MPa)
FeF ₃ /M ₁ AB ₄	140.4	1053	8.281	1.556
FeF ₃ /M ₂ AB ₃	106.9	3809	10.39	1.182
FeF ₃ /M ₃ AB ₂	389.8	374.4	2.882	0.8184
FeF ₃ /M ₄ AB ₁	223.6	537.0	5.081	0.9611

Figure 7 shows the discharge capacity after fixing the carbon material added to FeF₃ at 5 wt% and introducing AB and MWCNTs at various ratios. When the cutoff voltage was set as 0.5 V, it was confirmed that all samples except the FeF₃/M₂AB₃ sample had a discharge capacity of 500–550 mAh/g, which was 70–77% of the theoretical capacity of FeF₃ (712 mAh/g). Figure 8 shows the activation energy obtained from the TGA data shown in Figure 6. The formula for calculating the activation energy is as follows:

$$\log \frac{-\log(1-\alpha)}{T^2} = \log \frac{AR}{\beta E_a} \left(1 - \frac{2RT}{E_a} \right) - \frac{E_a}{2.303RT} \quad (7)$$

where α is the fraction of the sample decomposed at time t , given by

$$\alpha = \frac{W_i - W_t}{W_i - W_f} \quad (8)$$

β is the linear heating rate, T is the absolute temperature (K), E_a is the activation energy (K), A is the frequency factor, R is the gas constant 8.314 J/mol·K, w_i is the initial weight, w_t is the weight at a given temperature, and w_f is the final weight after completion of the reaction.

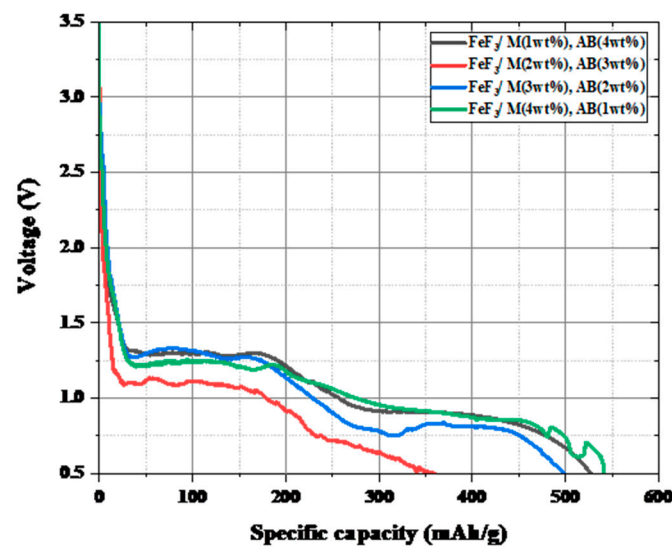


Figure 7. Discharge data for FeF_3 composite with AB and MWCNTs at different ratios.

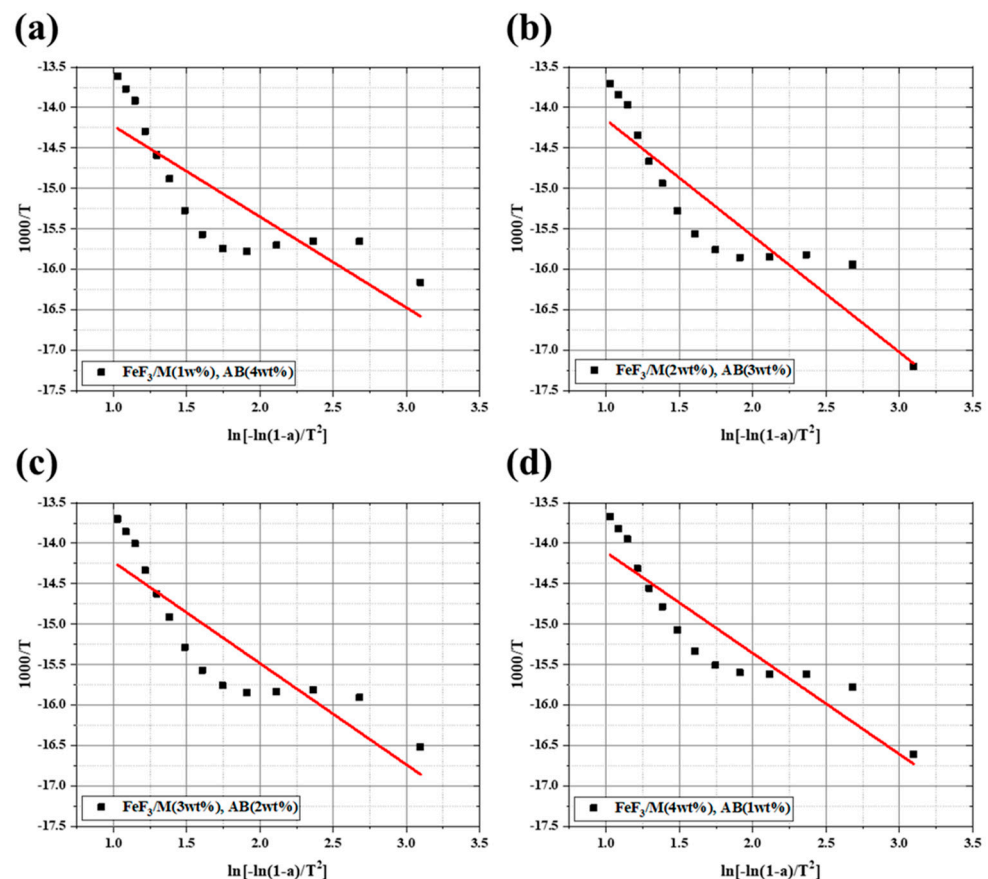


Figure 8. Activation energy of FeF_3 composite with AB and MWCNTs at different ratios. (a) $\text{FeF}_3/\text{M}_1/\text{AB}_4$; (b) $\text{FeF}_3/\text{M}_2/\text{AB}_3$; (c) $\text{FeF}_3/\text{M}_3/\text{AB}_2$; (d) $\text{FeF}_3/\text{M}_4/\text{AB}_1$.

The activation energy was calculated to account for the intercalation and discharge efficiency of Li^+ ions. The activation energy of $\text{FeF}_3/\text{M}_1/\text{AB}_4$, $\text{FeF}_3/\text{M}_2/\text{AB}_3$, $\text{FeF}_3/\text{M}_3/\text{AB}_2$, and $\text{FeF}_3/\text{M}_4/\text{AB}_1$ was 20.57, 26.33, 22.95, and 22.88 J/mol, respectively. The low activation energy indicated that the movement path of Li^+ was short. When the Li^+ movement distance was short, the Li^+ intercalation and discharge efficiencies increased [39,40]. The sample with the lowest activation energy was the $\text{FeF}_3/\text{M}_1/\text{AB}_4$ sample, which also had the highest discharge capacity, apart from the $\text{FeF}_3/\text{M}_4/\text{AB}_1$ sample. However, the

FeF₃/M₄/AB₁ sample was unstable in the low-voltage section. Therefore, considering the electrical conductivity, mechanical strength, discharge capacity, activation energy, and thermal stability, it can be concluded that FeF₃/M₁/AB₄ had the most suitable ratio of AB to MWCNTs. The discharge capacity and speed of a thermal battery depend on the microstructure and shape of the electrode, in addition to the unique physicochemical properties of the electrode material [41–43]. Because the capacity of a battery has a complex relationship with its components, the ratio of the FeF₃ composite in this study could not be considered perfect. However, by giving FeF₃ electrical conductivity, it showed its potential as a thermal battery cathode active material, and further research is needed to determine whether FeF₃ can perform better as a thermal battery cathode active material through complex formation with other carbon materials or metal plating. Consequently, this experimental result shows the potential as a cathode active material that can overcome the drawbacks of FeS₂, which is currently used as a thermal battery cathode active material.

4. Conclusions

To use FeF₃, which has high energy density but low electrical conductivity, as the active material for a thermal battery cathode, composites of FeF₃ with AB and MWCNTs were prepared. The ratio of the carbon material was varied from 2.5 wt% to 20 wt%, confirming that 5 wt% was the most suitable ratio. The composite of FeF₃ with both AB and MWCNTs exhibited advantages in terms of the electrical conductivity, mechanical strength, and discharge capacity. The composite afforded a discharge capacity of approximately 74% compared with the theoretical capacity of 712 mAh/g of FeF₃. Regarding using FeF₃ as a thermal battery cathode active material, the thermal stability could not be explained by a half cell using LiPF₆. However, discharge experiments were conducted using FeF₃ and carbon materials without using an organic binder so that it could be used immediately without additional processes when used in a thermal battery. Additionally, TGA data were used to demonstrate stability in the thermal battery operating environment. Therefore, the FeF₃/AB/MWCNT composite showed sufficient stability to be used as a cathode active material at high temperatures, which is the operating environment of a thermal battery. Considering the electrical conductivity, mechanical strength, discharge capacity, activation energy, and thermal stability, it was confirmed that FeF₃/M₁/AB₄ (1 wt.% MWCNTs and 4% AB) had the optimal ratio of AB and MWCNTs. The FeF₃ composite was fabricated by mixing AB and MWCNTs, and the characteristics of the composites with specific ratios were compared. This demonstrated the possibility of using the FeF₃/M₁/AB₄ composite as the active material for a thermal battery cathode.

Author Contributions: S.H.K. and J.-H.C. contributed equally to this work; conceptualization, S.H.K., J.-H.C. and S.H.P.; data curation, S.H.K., J.-H.C., S.H.P. and T.Y.A.; writing—original draft preparation, S.H.K. and J.-H.C.; writing—review and editing, S.H.K., J.-H.C., H.-W.C. and Y.S.Y.; supervision, H.-W.C. and Y.S.Y. All authors have read and agreed to the published version of the manuscript.

Funding: This work was supported by the Agency for Defense Development by the Korean Government (UI2200341D).

Data Availability Statement: Not applicable.

Conflicts of Interest: The authors declare no conflict of interest.

References

1. Ko, J.; Kang, S.H.; Cheong, H.W.; Yoon, Y.S. Recent Progress in Cathode Materials for Thermal Batteries. *J. Korean Ceram. Soc.* **2019**, *56*, 233–255. [[CrossRef](#)]
2. Kim, I.Y.; Woo, S.P.; Ko, J.; Kang, S.H.; Yoon, Y.S.; Cheong, H.W.; Lim, J.H. Binder-Free Cathode for Thermal Batteries Fabricated Using FeS₂ Treated Metal Foam. *Front. Chem.* **2020**, *7*, 904. [[CrossRef](#)] [[PubMed](#)]
3. Guidotti, R.A.; Masset, P. Thermally Activated (“thermal”) Battery Technology. Part I: An Overview. *J. Power Sources* **2006**, *161*, 1443–1449. [[CrossRef](#)]
4. Roh, H.C.; Kim, I.Y.; Ahn, T.Y.; Cheong, H.W.; Yoon, Y.S. Influence of Temperature on Performance of CuV₂O₆ Cathode for High Voltage Thermal Battery. *J. Korean Ceram. Soc.* **2021**, *58*, 507–518. [[CrossRef](#)]

5. Ko, J.; Kim, I.Y.; Jung, H.M.; Cheong, H.; Yoon, Y.S. Thin Cathode for Thermal Batteries Using a Tape-Casting Process. *Ceram. Int.* **2017**, *43*, 5789–5793. [[CrossRef](#)]
6. Masset, P.; Guidotti, R.A. Thermal Activated (Thermal) Battery Technology. Part II. Molten Salt Electrolytes. *J. Power Sources* **2007**, *164*, 397–414. [[CrossRef](#)]
7. Masset, P.J.; Guidotti, R.A. Thermal Activated (“thermal”) Battery Technology. Part IIIb. Sulfur and Oxide-Based Cathode Materials. *J. Power Sources* **2008**, *178*, 456–466. [[CrossRef](#)]
8. Zheng, X.; Zhu, Y.; Sun, Y.; Jiao, Q. Hydrothermal Synthesis of MoS₂ with Different Morphology and Its Performance in Thermal Battery. *J. Power Sources* **2018**, *395*, 318–327. [[CrossRef](#)]
9. Yang, T.; Cai, L.; White, R.E. Mathematical Modeling of the LiAl/FeS₂ High Temperature Battery System. *J. Power Sources* **2012**, *201*, 322–331. [[CrossRef](#)]
10. Liu, G.; Jiang, J.; Wang, X.; Tang, C.; Cui, Y.; Zhuang, Q. Al₂O₃ Nanoparticles Modified the FeS₂ Cathode to Boost the Interface Wettability and Electrochemical Performance for Thermal Batteries. *Mater. Lett.* **2023**, *330*, 133290. [[CrossRef](#)]
11. Au, M. Nanostructured Thermal Batteries with High Power Density. *J. Power Sources* **2003**, *115*, 360–366. [[CrossRef](#)]
12. Hu, J.; Zhao, L.; Chu, Y.; Tian, Q.; Wang, J.; Li, Y.; Wu, Q.; Zhu, Y. Preparation and Electrochemical Properties of a New Fe_{0.5}Co_{0.5}S₂ Cathode Material for Thermal Batteries. *J. Alloys Compd.* **2018**, *762*, 109–114. [[CrossRef](#)]
13. Tian, Q.; Hu, J.; Zhang, S.; Han, X.; Guo, H.; Tang, L.; Wang, J.; Hu, W. Scalable Preparation and Improved Discharge Properties of FeS₂@CoS₂ Cathode Materials for High-Temperature Thermal Battery. *Nanomaterials* **2022**, *12*, 1360. [[CrossRef](#)] [[PubMed](#)]
14. Masset, P.J.; Guidotti, R.A. Thermal Activated (“thermal”) Battery Technology. Part IIIa: FeS₂ Cathode Material. *J. Power Sources* **2008**, *177*, 595–609. [[CrossRef](#)]
15. Luo, Z.; Lin, X.; Tang, L.; Feng, Y.; Gui, Y.; Zhu, J.; Yang, W.; Li, D.; Zhou, L.; Fu, L. Novel NiCl₂ Nanosheets Synthesized via Chemical Vapor Deposition with High Specific Energy for Thermal Battery. *ACS Appl. Mater. Interfaces* **2020**, *12*, 34755–34762. [[CrossRef](#)]
16. Jin, C.; Zhou, L.; Fu, L.; Zhu, J.; Li, D. Synthesis and Discharge Performances of NiCl₂ by Surface Modification of Carbon Coating as Cathode Material of Thermal Battery. *Appl. Surf. Sci.* **2017**, *402*, 308–313. [[CrossRef](#)]
17. Giagloglou, K.; Payne, J.L.; Crouch, C.; Gover, R.K.B.; Connor, P.A.; Irvine, J.T.S. Transition Metal Chlorides NiCl₂, KNiCl₃, Li₆VCl₈ and Li₂MnCl₄ as Alternative Cathode Materials in Primary Li Thermal Batteries. *J. Electrochem. Soc.* **2018**, *165*, A3510–A3516. [[CrossRef](#)]
18. Guo, S.N.; Guo, H.; Wang, X.; Zhu, Y.; Hu, J.; Yang, M.; Zhao, L.; Wang, J. Iron Trifluoride as a High Voltage Cathode Material for Thermal Batteries. *J. Electrochem. Soc.* **2019**, *166*, A3599–A3605. [[CrossRef](#)]
19. Chang, Q.; Luo, Z.; Fu, L.; Zhu, J.; Yang, W.; Li, D.; Zhou, L. A New Cathode Material of NiF₂ for Thermal Batteries with High Specific Power. *Electrochim. Acta* **2020**, *361*, 137051. [[CrossRef](#)]
20. Dai, J.; Lai, M.; LaFollette, R.M.; Reisner, D. Thin Film Copper Vanadium Oxide Electrodes for Thermal Batteries. *ECS Trans.* **2011**, *33*, 3–9. [[CrossRef](#)]
21. Hillel, T.; Ein-Eli, Y. Copper Vanadate as Promising High Voltage Cathodes for Li Thermal Batteries. *J. Power Sources* **2013**, *229*, 112–116. [[CrossRef](#)]
22. Zhang, N.; Xiao, X.; Pang, H. Transition Metal (Fe, Co, Ni) Fluoride-Based Materials for Electrochemical Energy Storage. *Nanoscale Horiz.* **2019**, *4*, 99–116. [[CrossRef](#)] [[PubMed](#)]
23. Du, K.; Tao, R.; Guo, C.; Li, H.; Liu, X.; Guo, P.; Wang, D.; Liang, J.; Li, J.; Dai, S.; et al. In-Situ Synthesis of Porous Metal Fluoride@carbon Composite via Simultaneous Etching/Fluorination Enabled Superior Li Storage Performance. *Nano Energy* **2022**, *103*, 107862. [[CrossRef](#)]
24. Zhang, W.; Duchesne, P.N.; Gong, Z.L.; Wu, S.Q.; Ma, L.; Jiang, Z.; Zhang, S.; Zhang, P.; Mi, J.X.; Yang, Y. In Situ Electrochemical XAFS Studies on an Iron Fluoride High-Capacity Cathode Material for Rechargeable Lithium Batteries. *J. Phys. Chem. C* **2013**, *117*, 11498–11505. [[CrossRef](#)]
25. Wygant, B.R.; Merrill, L.C.; Harrison, K.L.; Talin, A.A.; Ashby, D.S.; Lambert, T.N. The Role of Electrolyte Composition in Enabling Li Metal-Iron Fluoride Full-Cell Batteries. *Adv. Sci.* **2022**, *9*, 2105803. [[CrossRef](#)]
26. Ko, J.; Yoon, Y.S. Functional Materials for Modifying Interfaces between Solid Electrolytes and Lithium Electrodes of All-Solid-State Lithium Metal Batteries. *J. Korean Ceram. Soc.* **2023**, *60*, 591–613. [[CrossRef](#)]
27. Liu, L.; Guo, H.; Zhou, M.; Wei, Q.; Yang, Z.; Shu, H.; Yang, X.; Tan, J.; Yan, Z.; Wang, X. A Comparison among FeF₃·3H₂O, FeF₃·0.33H₂O and FeF₃ Cathode Materials for Lithium Ion Batteries: Structural, Electrochemical, and Mechanism Studies. *J. Power Sources* **2013**, *238*, 501–515. [[CrossRef](#)]
28. Kim, S.H.; Jo, J.H.; Park, D.Y.; Moon, D.G.; Yoon, Y.S. Characteristics of La-Doped BSO(LBSO) Transparent Conductive Oxide as a Hole Transport Layer. *J. Korean Ceram. Soc.* **2022**, *59*, 631–637. [[CrossRef](#)]
29. Ko, J.; Kim, I.Y.; Cheong, H.; Yoon, Y.S. Organic Binder-Free Cathode Using FeS₂-MWCNTs Composite for Thermal Batteries. *J. Am. Ceram. Soc.* **2017**, *100*, 4435–4441. [[CrossRef](#)]
30. Ago, H.; Kugler, T.; Cacialli, F.; Salaneck, W.R.; Shaffer, M.S.P.; Windle, A.H.; Friend, R.H. Work Functions and Surface Functional Groups of Multiwall Carbon Nanotubes. *J. Phys. Chem. B* **1999**, *103*, 8116–8121. [[CrossRef](#)]
31. Yabuuchi, N.; Sugano, M.; Yamakawa, Y.; Nakai, I.; Sakamoto, K.; Muramatsu, H.; Komaba, S. Effect of Heat-Treatment Process on FeF₃ Nanocomposite Electrodes for Rechargeable Li Batteries. *J. Mater. Chem.* **2011**, *21*, 10035–10041. [[CrossRef](#)]

32. Ballav, N.; Biswas, M. Conducting Composites of Polythiophene and Polyfuran with Acetylene Black. *Polym. Int.* **2005**, *54*, 725–729. [[CrossRef](#)]
33. Avilés, F.; Cauich-Rodríguez, J.V.; Moo-Tah, L.; May-Pat, A.; Vargas-Coronado, R. Evaluation of Mild Acid Oxidation Treatments for MWCNT Functionalization. *Carbon* **2009**, *47*, 2970–2975. [[CrossRef](#)]
34. Jiang, Z.; Jin, J.; Xiao, C.; Li, X. Effect of Surface Modification of Carbon Black (CB) on the Morphology and Crystallization of Poly(Ethylene Terephthalate)/CB Masterbatch. *Colloids Surf. A Physicochem. Eng. Asp.* **2012**, *395*, 105–115. [[CrossRef](#)]
35. Yap, H.W.; Lakes, R.S.; Carpick, R.W. Mechanical Instabilities of Individual Multiwalled Carbon Nanotubes under Cyclic Axial Compression. *Nano Lett.* **2007**, *7*, 1149–1154. [[CrossRef](#)]
36. Liu, X.M.; Huang, Z.D.; Oh, S.W.; Zhang, B.; Ma, P.C.; Yuen, M.M.F.; Kim, J.K. Carbon Nanotube (CNT)-Based Composites as Electrode Material for Rechargeable Li-Ion Batteries: A Review. *Compos. Sci. Technol.* **2012**, *72*, 121–144. [[CrossRef](#)]
37. Guoping, W.; Qingtang, Z.; Zuolong, Y.; Meizheng, Q. The Effect of Different Kinds of Nano-Carbon Conductive Additives in Lithium Ion Batteries on the Resistance and Electrochemical Behavior of the LiCoO₂ Composite Cathodes. *Solid. State Ion.* **2008**, *179*, 263–268. [[CrossRef](#)]
38. Choi, Y.; Cho, S.; Lee, Y.S. Effect of the Addition of Carbon Black and Carbon Nanotube to FeS₂ Cathode on the Electrochemical Performance of Thermal Battery. *J. Ind. Eng. Chem.* **2014**, *20*, 3584–3589. [[CrossRef](#)]
39. Yang, S.; Yan, B.; Wu, J.; Lu, L.; Zeng, K. Temperature-Dependent Lithium-Ion Diffusion and Activation Energy of Li_{1.2}Co_{0.13}Ni_{0.13}Mn_{0.54}O₂ Thin-Film Cathode at Nanoscale by Using Electrochemical Strain Microscopy. *ACS Appl. Mater. Interfaces* **2017**, *9*, 13999–14005. [[CrossRef](#)]
40. Okubo, M.; Tanaka, Y.; Zhou, H.; Kudo, T.; Honma, I. Determination of Activation Energy for Li Ion Diffusion in Electrodes. *J. Phys. Chem. B* **2009**, *113*, 2840–2847. [[CrossRef](#)]
41. Zhang, X.; Wang, C.; He, K.; Zhang, X.; Cao, Y.; Xie, Y.; Cui, Y.; Liu, X.; Zeng, C. Transport Performance of Molten Salt Electrolyte in a Fractal Porous FeS₂ Electrode: Mesoscale Modeling and Experimental Characterization. *ACS Appl. Energy Mater.* **2021**, *4*, 14363–14371. [[CrossRef](#)]
42. Humplik, T.; Stirrup, E.K.; Grillet, A.M.; Grant, R.P.; Allen, A.N.; Wesolowski, D.E.; Roberts, C.C. Quantification of Ionic Transport within Thermally-Activated Batteries Using Electron Probe Micro-Analysis. *J. Power Sources* **2016**, *320*, 343–348. [[CrossRef](#)]
43. Reinholz, E.L.; Roberts, S.A.; Schunk, P.R.; Apblett, C.A. Mesoscale Modeling and Simulation of Composition, Manufacturing, and Microstructure Effects on Electrical Conduction in Thermal Battery Cathodes. *ECS Trans.* **2015**, *69*, 37–43. [[CrossRef](#)]

Disclaimer/Publisher’s Note: The statements, opinions and data contained in all publications are solely those of the individual author(s) and contributor(s) and not of MDPI and/or the editor(s). MDPI and/or the editor(s) disclaim responsibility for any injury to people or property resulting from any ideas, methods, instructions or products referred to in the content.